

Transition Metals Trigger On-Surface Ullmann Coupling Reaction: Intermediate, Catalyst and Template

L. Dong, S. Wang, W. Wang, C. Chen, T. Lin, J. Adisojoso
and N. Lin

Abstract In this chapter, we report on our recent studies of on-surface Ullmann coupling reaction and focus on the roles of the transition metals in the reaction. First, we discuss an organometallic intermediate state, which separates the reaction into two steps. Next, we examine the catalytic efficiency of Cu, Au, Ag, Pt, and Pd in the reaction. We analyze the bond formation yields when the reaction takes place in the presence of these metals. In particular, we determine the rate constants and activation energy of Cu- and Pd-catalyzed reaction. In the last part, we demonstrate a strategy of using metal coordination template to steer the reaction toward specific products.

1 Introduction

Molecular self-assembly on surfaces is a fundamental strategy for the bottom-up fabrication of nanostructures [1]. Various intermolecular interactions such as van der Waals interaction [2], hydrogen bonds [3, 4], halogen bonds [5], and metal–organic coordination bonds [6] have been utilized to build nanostructures. Taking the advantage of the reversibility of such bonding, long-range-ordered organizations have been formed. However, such structures are inherently fragile due to the weak intermolecular interactions, which lead to poor mechanical stability and low charge-transport efficiency. Robust and irreversible covalent bonding offers a way to overcome these limitations. Ullmann reaction [7], the C–C coupling between halogen aromatics via catalysts, has been employed onto surface for the synthesis of covalent-linked oligomers and polymers. A wide range of one-dimensional (1D) [8–10] and two-dimensional (2D) [11–13] materials has been successfully obtained via this route. Moreover, on-surface chemistry under ultrahigh vacuum (UHV) allows a much

L. Dong · S. Wang · W. Wang · C. Chen · T. Lin · J. Adisojoso · N. Lin (✉)
Department of Physics, The Hong Kong University of Science and Technology,
Clear Water Bay, Kowloon, Hong Kong, China
e-mail: phnlin@ust.hk

broader range of reaction temperatures, and the 2D confined geometry could favor reactions not accessible in the three dimensional space. Many of these studies utilized scanning tunneling microscopy (STM), which is a powerful tool not only imaging at the sub-molecular level, but also revealing molecular orbitals. The active research in this field provides unprecedented insights into the reaction mechanism [14].

In this chapter, we report on the STM studies of Ullmann reaction taking place in the presence of different transition metals. These metal species are in the form either as substrate (*intrinsic*) or as deposit (*extrinsic*). Our focus is to understand the roles the transition metals play in the Ullmann reaction. In Sect. 2, we present a combined experimental and theoretical study which reveals topographic and electronic signatures of an organometallic intermediate state containing C–Cu–C moieties. In Sect. 3, we first analyze the activity of *intrinsic* Cu, Ag, and Au and *extrinsic* Pt catalysts and conclude that the catalytic efficiency in the two reaction steps is very different for different metals. Furthermore, we compare the pathways of the reaction catalyzed by *extrinsic* Cu and Pd catalysts and determine the activation energy quantitatively. In Sect. 4, we demonstrate a strategy of using metal coordination bonds as template to steer the Ullmann reaction, which allows us to control the on-surface polymerization processes toward size-limited macromolecular structures.

2 Organometallic Intermediate State

A typical Ullmann reaction generally involves multiple steps from the halogen-contained molecules to the final coupled product. In the surface-confined reaction path, an essential intermediate state has been proposed by several groups [13, 15–18]. The study of the formation and structure of this intermediate state can give us a better understanding of the reaction mechanisms and dynamics [14]. It has been proposed that the radicals in the intermediate were connected by molecule–molecule and surface–mediated interactions [16, 19]. A Cu-atom-linked intermediate was also suggested based on the distance between two neighboring radicals [15, 17].

2.1 Topographic Identification

Here, we used STM measurements and DFT calculations to identify an organometallic intermediate incorporating C–Cu–C bridges in the on-surface Ullmann reaction [20]. As illustrated in Fig. 1a, after the deposition to a Cu(111) surface kept at room temperature, molecules of 4,4"-dibromo-*p*-terphenyl (compound **1**) are completely debrominated resulting in a Cu-bridged polymeric organometallic intermediate; an annealing at 473 K triggers the C–C coupling with the Cu atoms released and poly(*para*-phenylene) oligomers formed.

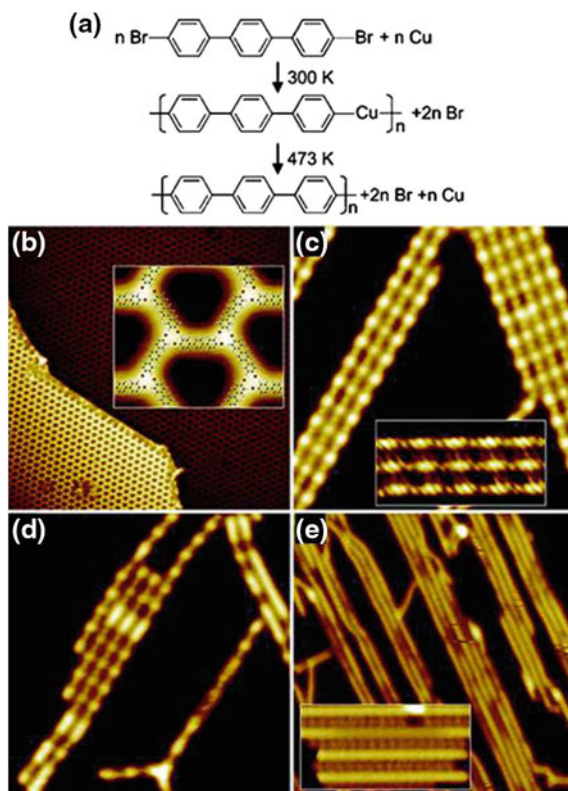


Fig. 1 **a** Surface-supported Ullmann coupling reaction path of compound **1** to poly(*para*-phenylene). **b** STM image of self-assembly of the molecules on Cu(111) at 77 K (120 nm \times 120 nm). *Inset* Magnified STM image of the network with molecular models superimposed (6 nm \times 5 nm). **c** STM image of the sample annealed to 300 K (20 nm \times 20 nm). *Inset* Br atoms trapped between the linear structures (8 nm \times 4 nm). **d** STM image of the sample annealed to 393 K (20 nm \times 20 nm). **e** STM image of sample annealed to 473 K (40 nm \times 40 nm). *Inset* Br atoms lying between the poly(*para*-phenylene) oligomers (8 nm \times 4 nm) [20]

As shown in Fig. 1b, the STM image reveals a honeycomb network on the Cu (111) surface at 77 K after the adsorption of **1**. A vortex structure is resolved at the joint of three molecules in the inset of Fig. 1b. With the molecular model superimposed, we can see that a terminal Br atom (in red) points toward an H atom of the neighboring molecule. The distance between the Br and the H atoms is 3.2 ± 0.5 Å. Therefore, we propose that the molecules are yet intact at 77 K and this molecular network is stabilized by Br...H–C hydrogen bonds. A 473 K annealing treatment destroyed the well-ordered honeycomb network and left newly formed linear chains (see Fig. 1e). No apparent periodicity was resolved in the chains. Electronic band structures of poly(*para*-phenylene) oligomers were observed [21]. Both topographic and electronic features indicate that these chains are poly(*para*-phenylene) oligomers, which means Ullmann coupling has successfully completed. Another

interesting feature is the small dots between the chains (inset of Fig. 1e). Similar features have been observed for iodine-aromatic systems adsorbed on Cu(110) surface and assigned as dissociated iodine atoms adsorbed on the surface [15]. It was reported that on Cu(111) surface Br atoms are dissociated from the phenyl group at 300 K [17]. We attribute these dots to be adsorbed Br atoms cleaved from the molecules.

After annealing at 300 K, the 2D honeycomb networks converted to linear structures (Fig. 1c). In comparison with the final product aforementioned, a periodic feature emerged in these linear structures. These linear structures are commensurate with the Cu lattice: each three periods matches 11 Cu atoms in the $[11\bar{2}]$ direction, that is, with a periodicity of 16.2 ± 0.2 Å. This distance is much larger than the length of a single debrominated $(\text{ph})_3$ unit, which is 11.4 Å as calculated by DFT. In contrast to the sample prepared at 77 K, Cu surface at room temperature provides sufficient 2D Cu adatom gas, which could be easily incorporated in the organometallic intermediate. We hence propose that the brighter oval features are $(\text{ph})_3$ biradicals that are connected by Cu adatoms. A DFT optimized linear periodic structure is shown in Fig. 2a. The side view of the structure reveals that the Cu atoms are almost in the same plane of the phenyl rings and do not bind strongly to the substrate.

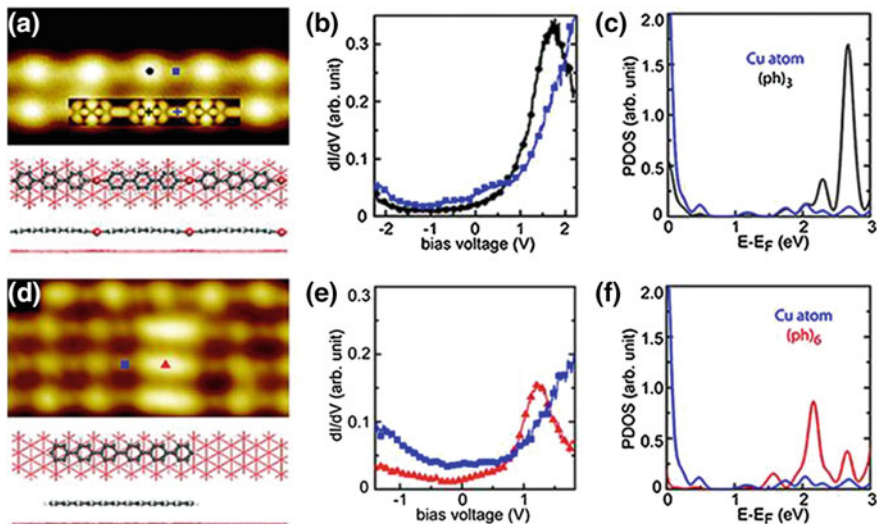


Fig. 2 **a** High-resolution STM image of the intermediate ($8 \text{ nm} \times 4 \text{ nm}$) and the DFT calculated structure. *Inset* simulated STM image at $+2.7 \text{ V}$. **b** dI/dV spectra measured at $(\text{ph})_3$ (black) and Cu (blue) sites marked in **a**. **c** Calculated PDOS of $(\text{ph})_3$ (black) and Cu (blue) in the inset of **a**. **d** STM image of the intermediate annealed to 393 K ($8 \text{ nm} \times 4 \text{ nm}$) and calculated structure. **e** and **f** Experimental dI/dV and PDOS of $(\text{ph})_6$ (red) and Cu (blue) in **d** [20]

2.2 Electronic Characterization and DFT Calculation

We conducted tunneling spectroscopic (dI/dV) measurements on the intermediate states. The $(\text{ph})_3$ part shows a prominent peak at +1.7 V, while the Cu atom shows only a gradual climbing state starting from +1.0 V (Fig. 2b), which is in good agreement with the calculated projected density of states (PDOS) in Fig. 2c, where the $(\text{ph})_3$ has an electronic state at +2.7 V while the Cu atom shows no apparent features (Fermi level is commonly offset in the DFT calculations). A simulated STM image of the intermediate at +2.7 V is shown in Fig. 2a which reproduces well the main features of the experimental results.

Between the intermediate and the final oligomer, furthermore, a mixed state was identified after an annealing of 393 K. As shown in Fig. 2d, besides the periodical features observed in Fig. 1c, bright segments of different length emerge in the linear structures, and the shortest one is identified with a length of 2.5 nm, equal to the dimension of a $(\text{ph})_6$ oligomer. In the dI/dV spectra shown in Fig. 2e, such a $(\text{ph})_6$ oligomer has a peak at +1.2 V, which is 0.5 V lower than main state of $(\text{ph})_3$, which is consistent with the isolated $(\text{ph})_6$ oligomer result [21]. The Cu atom shows similar feature as the intermediate case. In the calculated PDOS, the prominent peak of $(\text{ph})_6$ oligomer (+2.2 V) is 0.5 V lower than $(\text{ph})_3$ (Fig. 2f), which agrees well with the experimental values. On basis of both the topographic and electronic properties of the bright segments, we believe that they are short poly(*para*-phenylene) oligomers formed by covalent-linked $(\text{ph})_3$ units. The length of the poly(*para*-phenylene) oligomers $((\text{ph})_{3n})$ is shorter than the chain containing the same number (n) of $(\text{ph})_3$ units, implying the fact that Cu atoms are released during this transition.

Besides Cu, other transition metal atoms are also found to form organometallic intermediates including Ag [22] and Pt, which will be discussed later.

3 Transition Metal Catalysts

3.1 Intrinsic Ag, Au, Cu, and Extrinsic Pt Catalysts

In this part, we discuss a series of comparative experiments of Ullmann coupling of 1,3,5-tris(4-bromophenyl)benzene (compound **2**) molecules on fcc(111) transition metal surfaces of Ag, Au, and Cu. We also examined the catalytic behavior of *extrinsic* Pt deposits on Ag surface. As illustrated in Fig. 3, three distinct states can be identified by STM: an initial state of intact molecules (IS), an intermediate state of organometallic state (IntS), and a final state of covalently linked molecules (FS). We quantitatively analyzed the yields of the FS when the reaction was catalyzed by different catalysts.

It has been reported that deposition of **2** onto Cu(111) held at room temperature resulted in an IntS with C–Cu–C bond, but the deposition onto the substrate held at

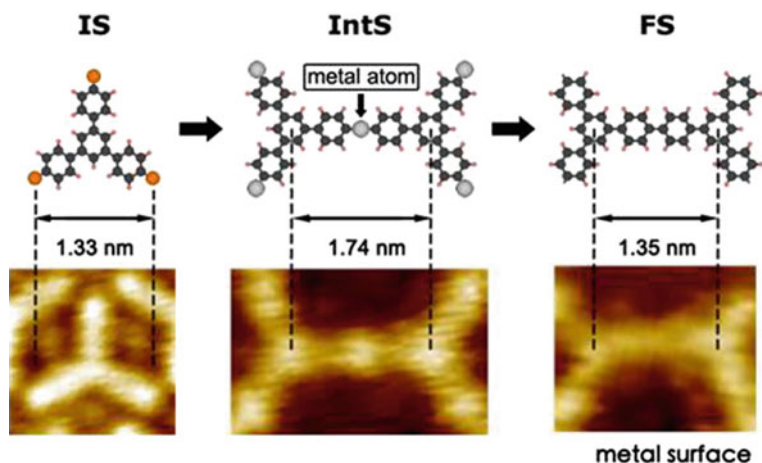


Fig. 3 Scheme of the on-surface Ullmann reaction path of **2** on Ag(111) surface with corresponding topographic structures in STM: IS to IntS to FS. Black C; Red H; Orange Br; Gray Ag

80 K kept the molecules intact [17]. Thus, the transition from IS to IntS occurs below the temperature of 300 K. Here, we focused on the transition from IntS to FS. We annealed the sample step-wisely to monitor when the conversion from the IntS to FS happens. As shown in Fig. 4a, after a 370 K annealing, the IntS developed into larger and regular organometallic networks stabilized by C–Cu–C bonds, indicating that the C–Cu–C bonds are quite stable at this temperature. Further annealing to 390 K disrupted the regular networks of the IntS and a small fraction of the IntS was converted into FS. The IntS-to-FS conversion became significant above 400 K and reached over 90 % at 410 K as shown in Fig. 4b.

Ullmann Coupling of **2** on Au(111) was reported by Blunt et al. [23], revealing that molecules are intact as deposited on a room-temperature sample, then form covalently coupled dimers at ~ 380 K and fully connected covalent networks at ~ 450 K. These results were reproduced in our study. Figure 4d shows that the IS (up-right corner) and the dimer phase coexisted after being heated to 370 K [23, 24]. Further annealing at 430 K led to irregular polymer network structures associated with the molecules fully converted to the FS (Fig. 4e). Differing from the Cu(111) case, we did not observe any IntS on the Au(111) surface in the temperature range between 300 and 450 K.

Walch et al. [17] reported that molecules **2** keep intact on Ag(111) surface at room temperature. Here, we examined its high-temperature behavior. As shown in Fig. 4g, after an annealing at 390 K, an open network structure consisting of polygons replaced the close-packed molecular monolayer formed at room temperature. The sides of the polygons consist of a pair of **2** linked in a head-to-head manner. The center-to-center distance between two neighboring molecules is about 1.74 nm with a protrusion in the middle. The distance indicates that this configuration is a C–Ag–C IntS [25]. We found that this C–Ag–C IntS was very robust

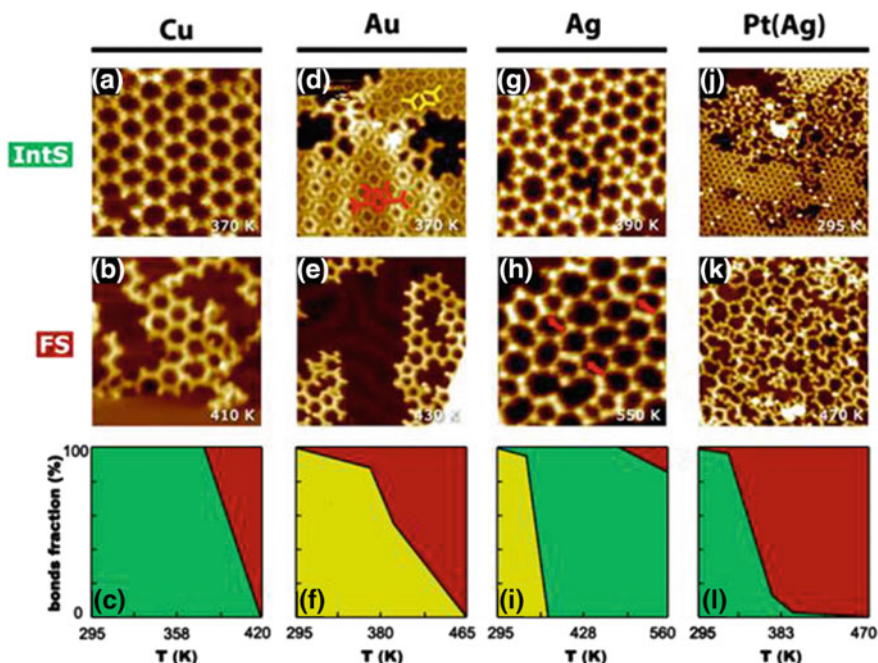


Fig. 4 STM images of the representative products and the bonds fraction in the reaction process on various metal surfaces: **a–c** Cu; **d–f** Au; **g–i** Ag; **j–l** Ag dosed with Pt. *Yellow* IS; *Green* IntS; *Red* FS. **a** and **b** 16.5 nm × 16.5 nm. **d** 14.4 nm × 14.4 nm. **e** 19.8 nm × 19.8 nm. **g** 18.9 nm × 18.9 nm. **h** 13.8 nm × 13.8 nm. **j** 23.0 nm × 23.0 nm. **k** 21.0 nm × 21.0 nm

against annealing. After 550 K heating, only 10 % of IntS was converted into FS (cf. Fig. 4h).

Based on the experimental observation, we analyzed the number of different types of bonds formed on the three substrates at various temperatures (from 295 K to 420, 465 and 560 K for Cu, Au, and Ag, respectively). The fraction of the three states, IS (yellow), IntS (green) and FS (red), is plotted in the bottom panels of Fig. 4. Apparently, the Ullmann reaction proceeds comparatively different on the three metals: (1) At 295 K, IS is present on Au and Ag but not on Cu, indicating that the IS is stable on Au(111) and Ag(111) but more reactive on Cu(111); (2) Cu and Ag form organometallic IntS but no Au organometallic species being observed, presumably C–Au–C is either unstable or having a short lifetime; (3) On Cu or Au, all molecules are converted into FS at 420 or 465 K, but the conversion is only ~10 % on Ag even at a much high temperature of 560 K.

Pt is a widely used catalyst in organic synthesis [26]. To explore the catalytic activity of Pt, we deposited Pt at Ag(111). As discussed before, on Ag(111) the yield of C–C bond formation is very low even upon 550 K annealing, hence Ag is an ideal surface for exploring the catalytic ability of Pt deposits. Figure 4j shows that after adding Pt at room temperature onto predeposited monolayer of **2**, the

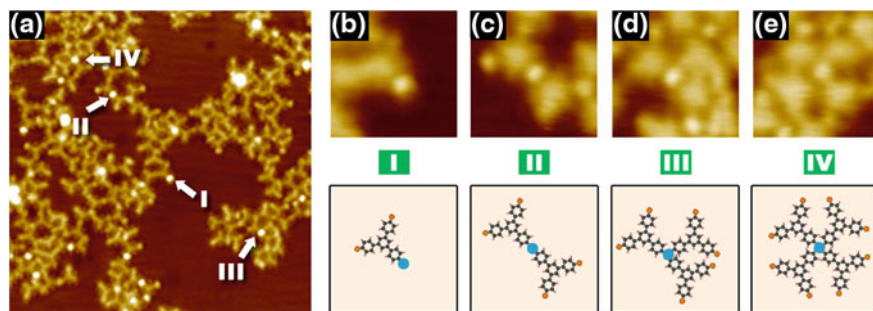


Fig. 5 a STM image of the IntS formed by Pt and **2**, which shows different coordination numbers for single Pt atom (25.4 nm \times 25.4 nm). b–e STM images with corresponding schematic models of Pt coordinated with 1, 2, 3 and 4 molecules, respectively (3.2 nm \times 3.2 nm)

close-packed monolayer is disrupted. One can see that lots of bright dots are scattered in the molecular layer. From the larger apparent height than Ag atom in the IntS, we attribute them to be Pt atoms. Figure 5a shows a STM topography of the sample after an annealing at 320 K. One can see that the bright dots are attached to the corners of the triangular shape molecules. Figure 5c shows that two monomers are linked by a dot in which the molecular center-to-center distance is 1.74 nm. This value agrees with an organometallic intermediate state containing C–Pt–C bonding. In contrast to the Ag or Cu linked organometallic states in which the metal atoms are always in a twofold coordination, the Pt atoms may coordinate to one, two, three, or four molecules. Figure 5b–e shows several such examples with the corresponding models illustrated in Fig. 5f–i. Further annealing at 380 K converted 90 % of the IntS into FS. Finally, annealing at 470 K achieved almost a 100 % conversion (cf. Fig. 4k). The temperature-dependent fraction of different states of Pt-catalyzed reaction is plotted in Fig. 4l. Compared to what happened on the pristine Ag surface, we conclude that Pt deposits significantly enhance the Ullmann reaction.

The yield of the Ullmann reaction, defined as the conversion ratio of the FS, catalyzed by the four metals is summarized in Fig. 6a. The ratios account for an overall catalytic activity sequence of Pt > Au > Cu > Ag. As we have aforementioned, the Ullmann reaction proceeds in two steps that are separated by the IntS. Based on the fractions of the three states shown in Fig. 4, we propose a qualitative energy diagram shown in Fig. 6b. The energy barrier I defines the conversion of IS to IntS. Upon deposition on the substrates held at room temperature, **2** is in IS on Ag and Au but completely forms IntS on Cu- and Ag-dosed with Pt. Thus, barrier I in the Cu- or the Pt-catalyzed reaction is lower than that in the Ag- or Au-catalyzed process. The barrier II defines converting the IntS to FS in the second step. Since Ag-stabilized organometallic state is stable up to 550 K, barrier II on Ag is the highest. On Au, because no IntS was detected, we assume that the barrier II is very low or absent.

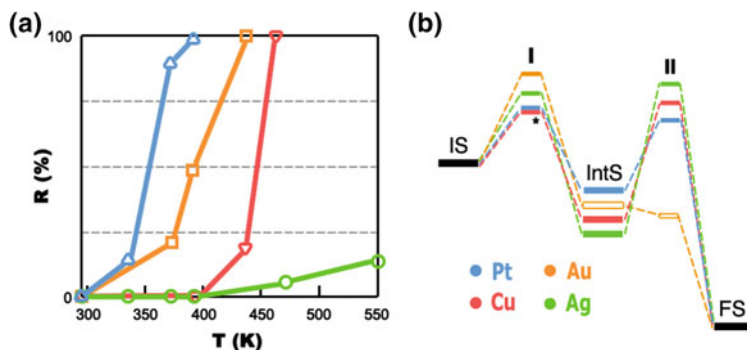


Fig. 6 **a** Conversion ratios defined in the text as a function of annealing temperatures for different transition metals. **b** Schematic energy diagram of the reaction process for all the metals

3.2 Extrinsic Pd and Cu Catalysts

We chose the polymerization reaction of 5,15-bis-(4-bromo-phenyl)-10,20-diphenyl porphyrin (compound **3**, see the inset of Fig. 7a) as our model system to investigate *extrinsic* Cu and Pd catalysts [27]. As a prototypical catalyst of Ullmann reaction, Cu catalysis is vital in the reaction process. Pd is the most

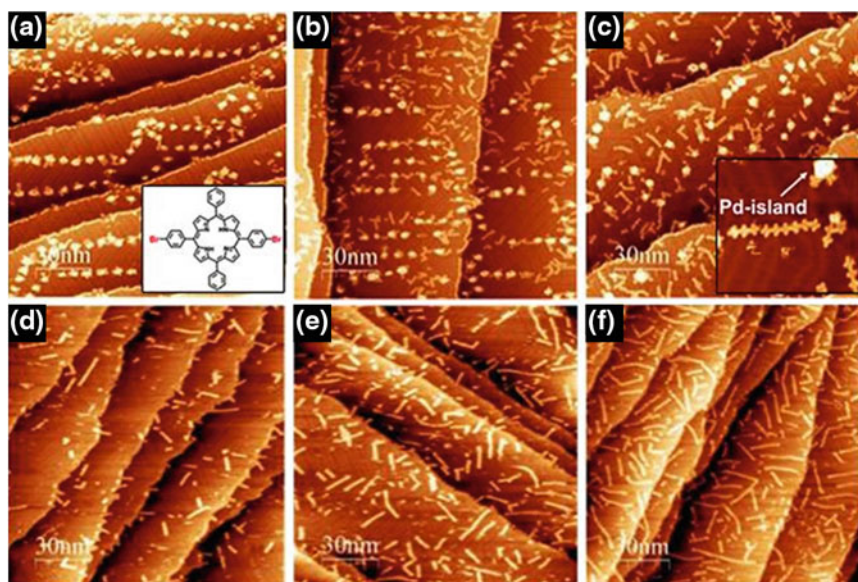


Fig. 7 **a–c** STM images of polymeric chains formed by **3** and Pd with annealing of 447 K for 5, 45, 105 min, respectively. *Inset* of **c** high-resolution STM image of the **3**-Pd chain (25 nm × 25 nm). **d–f** STM images of polymeric chains formed by **3** and Cu with annealing of 453 K for 5, 75, 160 min, respectively [27]

versatile catalyst used in homo-coupling and cross-coupling reactions [28, 29]. Here, we used STM to monitor the isothermal reaction and then determined the reaction yields, rate constants, and activation energy. In addition, kinetic Monte Carlo (KMC) simulation was utilized to explore the reaction mechanism.

After depositing **3** onto a Au(111) surface with predosed Pd, periodical chains were formed with a center-to-center distance of 1.74 ± 0.04 nm for the adjacent units, indicating covalently connected polymers (Fig. 7a–c). Similar chains were obtained when we conducted the Cu-catalyzed experiment on Au(111) surface (Fig. 7d–f). As contrast, annealing the same molecules on clean Au(111) up to 453 K for 30 min only gave us only 1.5 % covalently linked species, which confirms the catalytic influence of Pd or Cu on this Ullmann coupling reaction.

To study the reaction kinetics of C–C bond formation of **3** catalyzed by Pd, we annealed the sample at a defined temperature in 10–12 steps with 8–10 min for each. STM measurements were carried out after each step when the sample was cooled down to room temperature. The same procedure was conducted at different annealing temperatures. The discerning of dimers and even longer chains in STM images allows for the determination of the number of bonds formed as a function of reaction time and temperature. The increase of polymeric chains with longer reaction time is apparent in Fig. 7a–c, and this similar phenomenon was observed for each annealing temperature (Fig. 8). At higher temperatures, bond concentration rises rapidly until reaching a saturation value; At lower temperature, 393 K for example, a two-phase behavior emerges: A slow increase (0–60 min, defined as phase I) is followed by a rapid one (60–140 min, phase II). Such a two-phase behavior implies that the coupling reaction involves multiple steps. We suppose that phase I accounts for an initial activation process, and phase II is related to the C–C bond formation.

At higher temperature, e.g., 429 K, phase II is always the rate-limiting process while phase I is almost undetectable (Fig. 8a). As a result, by counting the number of formed C–C bond, activation energy could be calculated. We define [bond] and [phenyl–Br] as the concentration of the C–C bonds and intact phenyl–Br bonds, respectively, so the rate equation can be expressed as follows:

$$d[\text{bond}]/dt = k[\text{phenyl–Br}]^2 \quad (1)$$

Then the concentration of C–C bonds is given as:

$$[\text{bond}] = \frac{kt[\text{phenyl--Br}]_0^2}{1 + 2kt[\text{phenyl -- Br}]} + [\text{bond}]_0 \quad (2)$$

where [phenyl–Br]₀ and [bond]₀ refer to the initial concentration before the annealing.

In Fig. 8b, $\ln(k)$ versus T^{-1} is plotted according to the Arrhenius equation, where the k stands for the rate constant. By fitting the three reaction rate constants at higher temperature linearly, activation energy of (0.41 ± 0.03) eV and a prefactor of $(3 \times 10^{6 \pm 1}) \text{ s}^{-1} \text{ nm}^{-2}$ for the entire reaction are obtained. Since the much faster

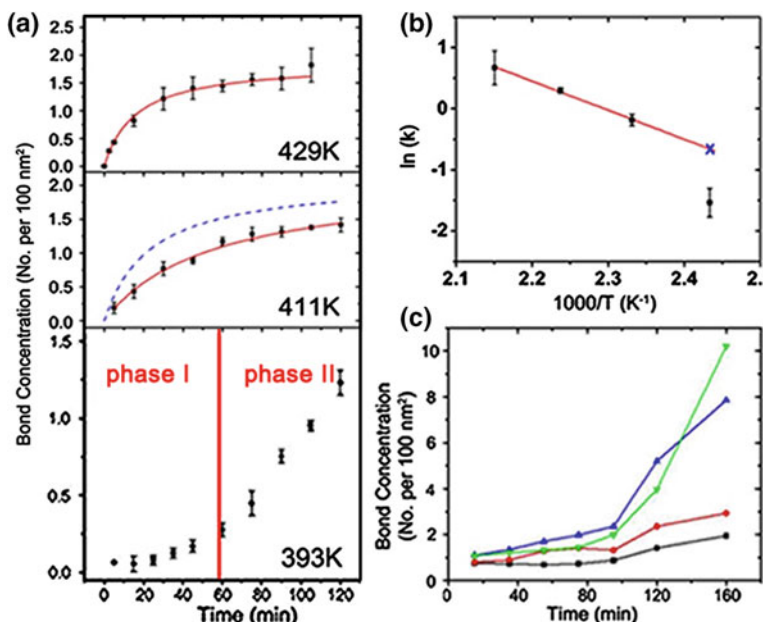


Fig. 8 **a** Bond concentration in Pd-catalyzed coupling of **3** on Au(111) as a function of reaction time at 393 K, 411 K, and 429 K. **b** Arrhenius plot of rate constant k obtained from experimental data. **c** Bond concentration in Cu-catalyzed coupling of **3** on Au(111) as a function of reaction time at 399 K (black), 417 K (red), 435 K (blue), and 453 K (green). The 453 K data are scaled down by a factor of five [27]

kinetics of phase I indicates an extremely low activation energy, the acquired value is more close to that of phase II alone. Considering the reported activation energy of the Ullmann coupling of iodobenzene on Cu(111) is 1.12 eV [30, 31], and the fact that iodine is more reactive than bromine, our result manifests the higher catalytic activity of Pd than Cu. At 411 K, phase I process cannot be neglected so the equations above are not completely suitable. A higher rate constant could be expected if we neglect phase I at that temperature, as the mark “x” in Fig. 8b, which corresponds to a bond concentration behavior described by the dashed curve in Fig. 8a. The lower value for the experimental bond concentration compared to this hypothesized one indicates the limiting effect of phase I at this temperature.

We found Pd and Cu result in distinct C–C bond formation yield and length distribution of the polymeric chains. When the initial molecule dosage was kept constant, at higher temperatures, Cu-catalyzed reactions show rapid increase (Fig. 8c) in the yield rather than the slight decline for Pd-catalyzed ones (Fig. 8a). Moreover, at specific temperature, Cu-catalyzed reaction always has a much higher yield and longer polymeric chains (Fig. 7), which is as well supported by the length distribution shown in Fig. 9a, b. Dimers are most favored in the Pd-catalyzed reactions with other chains no longer than hexamer, but no apparent length preference is observed in the Cu-catalyzed coupling.

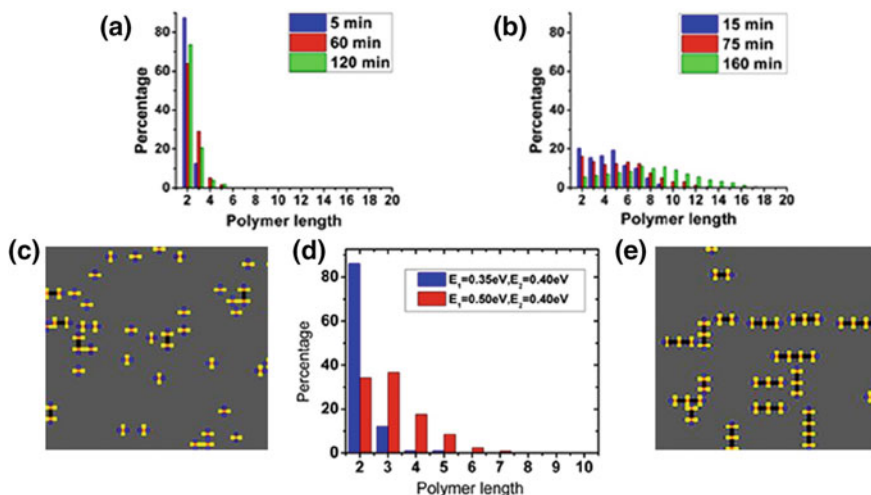


Fig. 9 Length distribution of the polymers catalyzed by **a** Pd at 465 K and **b** Cu at 453 K. **c** and **e** KMC simulated polymeric chains with $E_1 = 0.35$ eV and $E_1 = 0.50$ eV, whose length distributions are plotted in **d** [27]

For a better understanding of the difference between Pd and Cu, we carried out KMC simulations [32]. The reaction consists of two irreversible steps: the activation of a monomer's phenyl-Br bond with energy barrier E_1 , and the C-C bond formation with energy E_2 between an activated monomer and an inactivated one. According to our experimental results, E_1 was set to be larger for Cu (0.50 eV) than for Pd (0.35 eV), and E_2 was set at 0.40 eV for both. As shown in Fig. 9c, e, a lower E_1 leads to shorter chains. The distribution of polymeric length in the simulation illustrated in Fig. 9d is well reproduces the experimental observation. In the other aspect, the lower E_1 gives a lower yield (10.5 %) of C-C bonds than the higher one (67.7 %).

4 Metal-Coordination Template

Since the first surface-assisted realization of covalent-linked molecular nanostructure by polymerization via Ullmann coupling, as mentioned in the former sections, there has been a big challenge to control the final product. Due to the non-reversibility of covalent bonds, if kinetic trapping would be inevitably introduced in the polymerization processes, then it is difficult to control the size and distribution of the final macromolecular product on surface. Many effect has been made to eliminate this hindrance [33–38]. It was found that polycondensation of boronic acid could generate well-ordered covalent networks with the assistance of water [34, 35]. Gold surface with troughs was also exploited for the confinement

of alkene's polymerization [33]. Besides, molecules functionalized with different halogens were proved to be coupled step by step [38].

When “molecular and supramolecular science meet” [39], it brings out the template synthesis, that is, utilizing non-covalent structure to steer highly ordered covalent organization [40]. For the predesigned templates, various connections, including π - π interactions, hydrogen bond, and metal-ligand bond, have been adopted [41]. As we know, in comparison with covalent bond, coordination bond is less robust but reversible and specifically more flexible. In such consideration, we developed an effective approach of using metal-ligand coordination as template to steer the on-surface polymerization process. The resulting macromolecular structures exhibit a very narrow size distribution and are organized hierarchically through supramolecular assembly.

4.1 Verification of On-Surface Polymerization

Porphyrin derivatives with various end groups were utilized in our experiments [42]. The precursor of 5,15-bis-(4-bromophenyl)-10,20-diphenyl porphyrin (compound **4**) possesses both py(pyridine) groups as coordination sites for metal atoms and bromine groups for Ullmann coupling. It could form 1D metallorganic single-row (SR) chains with Cu atoms on a Au(111) surface at room temperature. In these SR chains, the adjacent molecules have a center-to-center separation of 1.9 nm, featuring py-Cu-py coordination bonds as the linkages (Fig. 10a) [43]. Cu atoms cannot be resolved probably due to electronic effects or tip conditions.

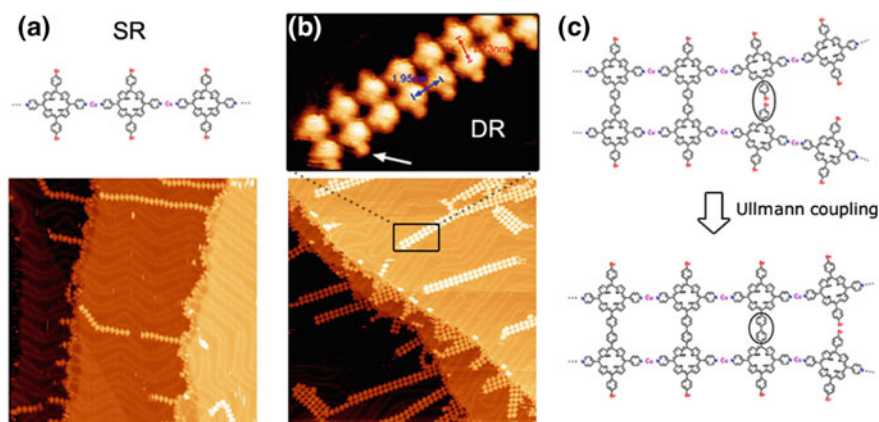


Fig. 10 **a** STM image of SR coordination chain formed from **4** and Cu on Au(111) surface at 298 K (100 nm \times 100 nm) with the proposed model. **b** STM image of DR and TR chains after annealing of 453 K (100 nm \times 100 nm), with a DR magnified. **c** Scheme of Ullmann coupling assisted by the py-Cu-py coordination template [42]

An annealing of 453 K for 30 min converted these SR chains to ladder-shaped double rows (DR) or triple rows (TR), as shown in Fig. 10b. A close inspection of the DR chain reveals two distinct center-to-center distances: 1.73 nm perpendicular to the chain (red arrow) and 1.95 nm along the chain (blue arrow). While the larger distance is the same as the SR case, the smaller distance is in good agreement with covalent-linked porphyrins. These structural characteristics clearly indicate that the DR chains consist of covalently bonded dimeric macromolecules linked by py–Cu–py coordination bonds along the chain direction, whose model is illustrated in Fig. 10c. It is also notable that there are small protrusions at the side of the chains pointed out with white arrow. These features have been observed on the SR chains and identified as bromine atoms. This phenomenon provides another piece of evidence that the molecules are arranged with their Br groups at the side in the DR chains. It is clear that 453 K annealing has already triggered the coupling of **4** forming covalent-linked dimers [5, 8, 9, 11, 12, 15, 38]. Such a lower activation temperature compared to the case on the pristine Au(111) surface is due to the catalytic effect of Cu.

4.2 Metal-Directed Template

To unravel the role of py functions, we carried out control experiments to explore the difference between **4** and **3** (see Sect. 3.2). Figure 11a shows the Au(111) surface deposited with **4** and Cu with an annealing of 453 K for 60 min. It shows

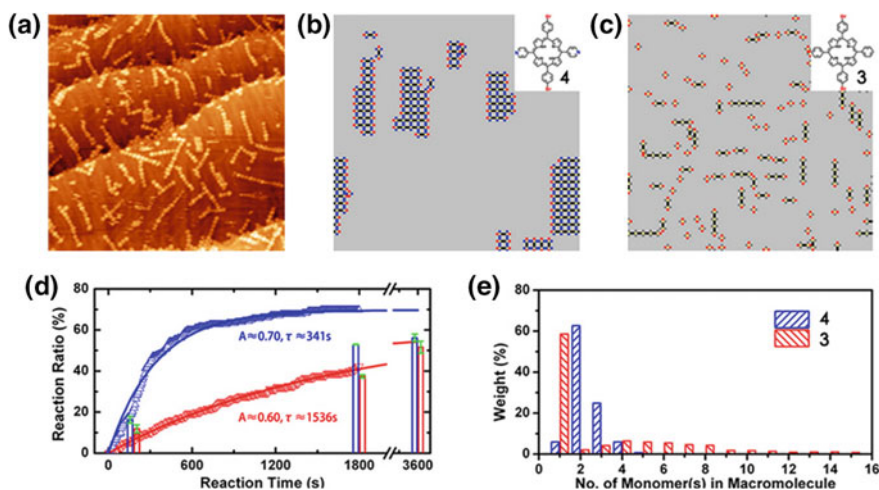


Fig. 11 Comparison of the polymerization of **4** and **3**. **a** STM image of SR chains formed from **3** (100 nm \times 100 nm). **b** and **c** KMC simulated structures formed out of **4** and **3**. **d** Reaction ratios of **4** and **3** as a function of reaction time. *Triangle* Simulation results. *Solid line* Exponential fittings. *Vertical bars* Experimental values. *Blue* **4**. *Red* **3**. **e** Experimental weight distribution of the macromolecular structures formed out of **4** and **3** as a function of the size of macromolecule [42]

covalently bonded polymeric chains [12]. Under the same Cu dosage and annealing treatment, we found that the reaction ratios of **3** were always lower than those of **4**, which can be seen from the vertical bars in Fig. 11d. We also conducted KMC simulation of **4** and **3** with Cu at 453 K for 30 min (Fig. 11b, c). For **4**, ladder-like structure is formed with py–Cu–py bonds in one direction (blue) and C–C covalent bond in the orthogonal direction (black). For **3**, only short single chains are generated. Moreover, most of **4** are involved in the coupled architecture, while about 60 % of **3** are adsorbing as isolated monomers. The simulated reaction ratios versus annealing time are plotted in Fig. 11d. With the fitting using function $A(1 - e^{-t/\tau})$, time constant could be obtained, and the value of **4** (341 s) is merely one-fifth of that of **3** (1536 s). However, the prefactor A is comparable for **3** and **4**. Therefore, the simulation verifies that the formation of coordination bonds can significantly enhance the coupling reaction rates.

Distribution of the macromolecular structures of certain sizes was also analyzed for the samples of **3** or **4** after 60-min annealing at 453 K, as shown in Fig. 11e. One can see that monomers account for 5 % in **4** but almost 60 % in **3**, reflecting the lower reaction rates of **3**. Apart from that, the macromolecular structures formed from **3** exhibit a much wider size distribution than from **4**. Majority of **4** (63 %) are coupled in dimeric configuration, and they are organized in order by coordination bonds in contrast to the random distribution of **3**.

Two possible mechanisms might take place during the reaction: (1) the SR chains are decomposed by the annealing and then the free monomers are coupled by covalent bonds. Coordination bonds reform as the sample is cooled down. However, such a process would generate macromolecules of a broad size distribution, and the final coordinated chains would be composed by them and have an inhomogeneous width. As this is not observed in the experiment, this presumption is ruled out. (2) A template-assisted coupling reaction as illustrated in Fig. 10c: a DR chain is grown from a dimeric molecule seed step by step. When two more monomers are anchored separately to the dimer via py–Cu–py bonds, to avoid the spatial conflict, those flexible bonds have to be bent as the model highlighted by circle in Fig. 10c, which could be found in the real structure as circled in Fig. 12b. In this configuration, the Br atoms are brought into proximity to facilitate the Ullmann coupling reaction as in topochemical polymerization processes [44]. According to our simulation, most C–C bonds were formed between the neighboring monomers anchored to the existing chains through coordination bonds; hence, we propose that Cu plays a dual role in promoting the C–C bond formation: One is reducing the reaction barrier as catalyst; one is ligating with py as template to speed up the reaction.

4.3 Size-Limited Polymerization

As discussed in the previous section, dimeric and trimeric chains predominate after the 453 K annealing, as shown in Figs. 10b and 11e. Different annealing temperatures were tested for the reaction of **4** and Cu. In Fig. 12a, it can be found that most of the

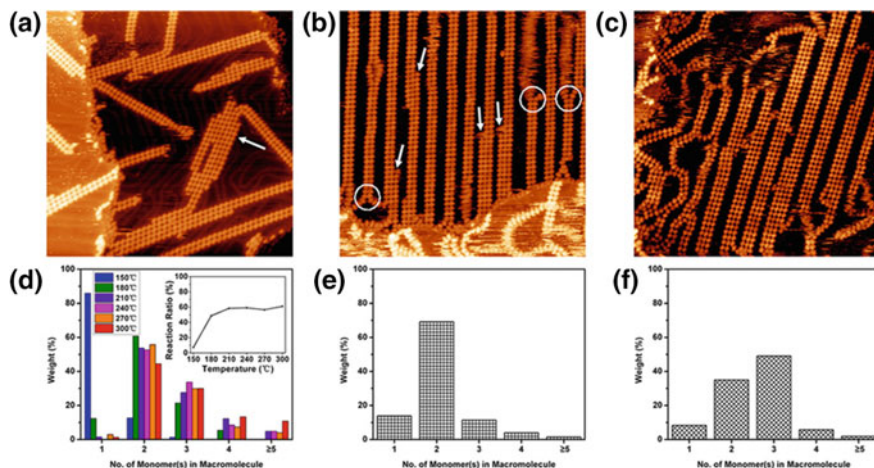


Fig. 12 STM images (100 nm \times 100 nm) and weight distribution of chains formed from **4** with different preparation parameters. **a** Molecules were deposited on Au(111) held at 298 K and annealed to 573 K. **b** Weight distribution with different annealing treatments. *Inset* the corresponding reaction ratio. **c** and **d** Deposition was done on the substrate held at 298 K and then annealed to 453 K. **e** and **f** Deposition was done on the substrate with precured Cu at 513 K [42]

products are DR chains after a 573 K annealing. The size distribution of the macromolecular structures produced at different annealing temperatures is plotted in Fig. 12d. The high-temperature annealing did not significantly enhance the formation of larger oligomers. Tetramers or larger ones are rarely observed, and the largest structure found is heptamer, as marked by the arrow in Fig. 12a. It is worth noting that DR chains are always the predominant structure when the annealing temperature is higher than 453 K.

Besides the size limitation, the chains always show very smooth edges. It implies that the attachment of individual monomers to the side of a chain is unfavorable, and even if it happens, a new row will grow along the side of the chain due to the template effect. In other word, the coordination template steered the polymerization process to favor the replication of the existing smaller (dimeric or trimeric) seed structures over the growth of larger structures, which led to the predominant formation of the dimeric macromolecules.

We prepared a sample with DR chains of low surface coverage, then put more Cu and **4** onto the surface with an additional annealing of 453 K for 30 min. As marked by arrows in Fig. 12b, some sections of several DR chains had been widened to TR chains. However, DR chains are still the main structures, as shown in the size distribution in Fig. 12e. Therefore, most of the lately added molecules either formed new DR chains or prolonged the existing ones, which is consistent with the proposed mechanism. It indicates that for a higher yield of wider chains, larger macromolecular structures must be generated at the early stage as seeds, which will grow longer via a self-replicating process. To verify this proposal, we deposited **4** onto a hot surface (513 K) predosed with Cu. More covalent-linked

trimers or larger macromolecules formed, which triggered the formation of wider chains, as shown in the STM image of Fig. 12c and the size distribution in Fig. 12f. The ratio of the TR chains reached 50 %, exceeding that of the DR chains.

5 Summary and Conclusions

In this chapter, we have discussed the roles of several transition metals in the on-surface Ullmann coupling reaction focusing on three aspects: (1) metal atoms form an organometallic intermediate in the reaction; (2) *intrinsic* metal substrates and *extrinsic* metal deposits catalyze the two reaction steps, and (3) metal-coordination template controls the polymerization via Ullmann coupling.

1. We have identified an organometallic state as an intermediate phase in the reaction. STM and DFT calculations revealed at a single-molecular level that the intermediate consists of biradical terphenyl (ph)₃ units that are connected by single Cu atoms through C–Cu–C bridges.
2. We have investigated the catalytic behavior of five transition metals of Ag, Pt, Au, Cu, and Pd. We found that Cu, Ag, and Pt form the organometallic intermediates. Based on statistical analysis of the yields of different species, we propose that the overall catalytic activity ranks as Pt > Au > Cu > Ag while the rate-limiting step varies with the different metals. By means of analyzing the isothermic series of Pd- and Cu-catalyzed reactions, we discovered that the two catalysts result in distinctive bond formation yields as well as reaction rates. We attribute these differences to the distinctive roles the two catalysts play in different reaction steps. We also determined the activation energy of Pd catalysis to be (0.41 ± 0.03) eV, which is lower than the Cu catalysis.
3. Using specially designed bifunctional porphyrin compounds, we have demonstrated that metal coordination can effectively alter the products of the on-surface polymerization. First, the dimeric structure is formed with a very high yield. Second, the macromolecules are organized by metal coordination into supramolecular chains on the surface. These results may shed lights on the design and synthesis of size- and shape-controlled macromolecular systems in the fast emerging field of on-surface synthesis.

The results presented in this chapter highlight the active roles that the transition metals play in the on-surface Ullmann reaction. We emphasize that in spite of the fact that this reaction is one of the most-studied on-surface reactions, more work must be done to get a better understanding as many open questions remain. For example, how does debromination occur? How to describe the molecules after debromination (radical might not be an accurate term)? How do the intermediate states form and convert to the final state? We believe that these questions are to be addressed for other on-surface reactions too.

References

1. Barth, J.V.: Molecular architectonic on metal surfaces. *Annu. Rev. Phys. Chem.* **58**, 375 (2007)
2. De Feyter, S., Miura, A., Yao, S., Chen, Z., Würthner, F., Jonkheijm, P., Schenning, A.P.H.J., Meijer, E.W., De Schryver, F.C.: Two-dimensional self-assembly into multicomponent hydrogen-bonded nanostructures. *Nano Lett.* **5**, 77 (2005)
3. Barth, J.V., Weckesser, J., Trimarchi, G., Vladimirova, M., De Vita, A., Cai, C., Brune, H., Günter, P., Kern, K.: Stereochemical effects in supramolecular self-assembly at surfaces: 1-D versus 2-D enantiomorphic ordering for PVBA and PEBA. *J. Am. Chem. Soc.* **124**, 7991 (2002)
4. Cañas Ventura, M.E., Xiao, W., Wasserfallen, D., Müllen, K., Brune, H., Barth, J.V., Fasel, R.: Self-assembly of periodic bicomponent wires and ribbons. *Angew. Chem. Int. Ed.* **46**, 1814 (2007)
5. Berger, G., Soubhye, J., Meyer, F.: Halogen bonding in polymer science: from crystal engineering to functional supramolecular polymers and materials. *Polym. Chem.* **6**, 3559 (2015)
6. Stepanow, S., Lin, N., Barth, J.V.: Modular assembly of low-dimensional coordination architectures on metal surfaces. *J. Phys. Cond. Mat.* **20**, 184002 (2008)
7. Ullmann, F., Bielecki, J.: Ueber Synthesen in der Biphenylreihe. *Ber. Dtsch. Chem. Ges.* **34**, 2174 (1901)
8. Grill, L., Dyer, M., Lafferentz, L., Persson, M., Peters, M.V., Hecht, S.: Nano-architectures by covalent assembly of molecular building blocks. *Nature Nanotech.* **2**, 687 (2007)
9. Lipton Duffin, J.A., Miwa, J.A., Kondratenko, M., Cicoira, F., Sumpter, B.G., Meunier, V., Perepichka, D.F., Rosei, F.: Step-by-step growth of epitaxially aligned polythiophene by surface-confined reaction. *PNAS* **107**, 11200 (2010)
10. Cai, J., Ruffieux, P., Jaafar, R., Bieri, M., Braun, T., Blankenburg, S., Muoth, M., Seitsonen, A.P., Saleh, M., Feng, X., Müllen, K., Fasel, R.: Atomically precise bottom-up fabrication of graphene nanoribbons. *Nature* **466**, 470 (2010)
11. Gutzler, R., Walch, H., Eder, G., Kloft, S., Heckl, W.M., Lackinger, M.: Surface mediated synthesis of 2D covalent organic frameworks: 1,3,5-tris(4-bromophenyl)benzene on graphite (001), Cu (111), and Ag (110). *Chem. Commun.* 4456 (2009)
12. Lafferentz, L., Eberhardt, V., Dri, C., Africh, C., Comelli, G., Esch, F., Hecht, S., Grill, L.: Controlling on-surface polymerization by hierarchical and substrate-directed growth. *Nature Chem.* **4**, 215 (2012)
13. Bieri, M., Nguyen, M.-T., Gröning, O., Cai, J., Treier, M., Ait-Mansour, K., Ruffieux, P., Pignedoli, C.A., Passerone, D., Kastler, M., Müllen, K., Fasel, R.: Two-dimensional polymer formation on surfaces: insight into the roles of precursor mobility and reactivity. *J. Am. Chem. Soc.* **132**, 16669 (2010)
14. El Garah, M., MacLeod, J.M., Rosei, F.: Covalently bonded networks through surface-confined polymerization. *Surf. Sci.* **613**, 6 (2013)
15. Lipton Duffin, J.A., Ivashenko, O., Perepichka, D.F., Rosei, F.: Synthesis of polyphenylene molecular wires by surface-confined polymerization. *Small* **5**, 592 (2009)
16. McCarty, G.S., Weiss, P.S.: Formation and manipulation of protopolymer chains. *J. Am. Chem. Soc.* **126**, 16772 (2004)
17. Walch, H., Gutzler, R., Sirtl, T., Eder, G., Lackinger, M.: Material-and orientation-dependent reactivity for heterogeneously catalyzed carbon-bromine bond homolysis. *J. Phys. Chem. C* **114**, 12604 (2010)
18. Blake, M.M., Nanayakkara, S.U., Claridge, S.A., Fernandez-Torres, L.C., Sykes, E.C.H., Weiss, P.S.: Identifying reactive intermediates in the Ullmann coupling reaction by scanning tunneling microscopy and spectroscopy. *J. Phys. Chem. A* **113**, 13167 (2009)

19. Sykes, E.C.H., Han, P., Kandel, S.A., Kelly, K.F., McCarty, G.S., Weiss, P.S.: Substrate-mediated interactions and intermolecular forces between molecules adsorbed on surfaces. *Acc. Chem. Res.* **36**, 945 (2003)
20. Wang, W., Shi, X., Wang, S., Van Hove, M.A., Lin, N.: Single-molecule resolution of an organometallic intermediate in a surface-supported ullmann coupling reaction. *J. Am. Chem. Soc.* **133**, 13264 (2011)
21. Wang, S., Wang, W., Lin, N.: Resolving band-structure evolution and defect-induced states of single conjugated oligomers by scanning tunneling microscopy and tight-binding calculations. *Phys. Rev. Lett.* **106**, 206803 (2011)
22. Chung, K.-H., Koo, B.-G., Kim, H., Yoon, J.K., Kim, J.-H., Kwon, Y.-K., Kahng, S.-J.: Electronic structures of one-dimensional metal-molecule hybrid chains studied using scanning tunneling microscopy and density functional theory. *Phys. Chem. Chem. Phys.* **14**, 7304 (2012)
23. Blunt, M.O., Russell, J.C., Champness, N.R., Beton, P.H.: Templating molecular adsorption using a covalent organic framework. *Chem. Comm.* **46**, 7157 (2010)
24. Russell, J.C., Blunt, M.O., Garfitt, J.M., Scurr, D.J., Alexander, M., Champness, N.R., Beton, P.H.: Dimerization of tri(4-bromophenyl)benzene by aryl-aryl coupling from solution on a gold surface. *J. Am. Chem. Soc.* **133**, 4220 (2011)
25. Park, J., Kim, K.Y., Chung, K.-H., Yoon, J.K., Kim, H., Han, S., Kahng, S.-J.: Interchain interactions mediated by Br adsorbates in arrays of metal-organic hybrid chains on Ag (111). *J. Phys. Chem. C* **115**, 14834 (2011)
26. Wintterlin, J., Volkening, S., Janssens, T., Zambelli, T., Ertl, G.: Atomic and macroscopic reaction rates of a surface-catalyzed reaction. *Science* **278**, 1931 (1997)
27. Adisoejoso, J., Lin, T., Shang, X.S., Shi, K.J., Gupta, A., Liu, P.N., Lin, N.: A single-molecule-level mechanistic study of Pd-catalyzed and Cu-catalyzed homocoupling of aryl bromide on an Au(111) surface. *Chem. Eur. J.* **20**, 4111 (2014)
28. Molnar, A.: Efficient, selective, and recyclable palladium catalysts in carbon-carbon coupling reactions. *Chem. Rev.* **111**, 2251 (2011)
29. Yin, L., Liebscher, J.: Carbon-carbon coupling reactions catalyzed by heterogeneous palladium catalysts. *Chem. Rev.* **107**, 133 (2007)
30. Nguyen, M.-T., Pignedoli, C.A., Passerone, D.: An ab initio insight into the Cu(111)-mediated Ullmann reaction. *Phys. Chem. Chem. Phys.* **13**, 154 (2011)
31. Meyers, J.M., Gellman, A.J.: Effect of substituents on the phenyl coupling reaction on Cu (111). *Surf. Sci.* **337**, 40 (1995)
32. Li, Y., Lin, N.: Combined scanning tunneling microscopy and kinetic Monte Carlo study on kinetics of Cu-coordinated pyridyl-porphyrin supramolecular self-assembly on a Au(111) surface. *Phys. Rev. B* **84**, 125418 (2011)
33. Zhong, D., Franke, J.-H., Podiyanachari, S.K., Blömker, T., Zhang, H., Kehr, G., Erker, G., Fuchs, H., Chi, L.: Linear alkane polymerization on a gold surface. *Science* **334**, 213 (2011)
34. Dienstaier, J.F., Medina, D.D., Dogru, M., Knochel, P., Bein, T., Heckl, W.M., Lackinger, M.: Isoreticular two-dimensional covalent organic frameworks synthesized by on-surface condensation of diboronic acids. *ACS Nano* **6**, 7234 (2012)
35. Dienstaier, J.F., Gigler, A.M., Goetz, A.J., Knochel, P., Bein, T., Lyapin, A., Reichlmaier, S., Heckl, W.M., Lackinger, M.: Synthesis of well-ordered COF monolayers: surface growth of nanocrystalline precursors *versus* direct on-surface polycondensation. *ACS Nano* **5**, 9737 (2011)
36. Guan, C.-Z., Wang, D., Wan, L.-J.: Construction and repair of highly ordered 2D covalent networks by chemical equilibrium regulation. *Chem. Comm.* **48**, 2943 (2012)
37. Weigelt, S., Bombis, C., Busse, C., Knudsen, M.M., Gothelf, K.V., Lægsgaard, E., Besenbacher, F., Linderoth, T.R.: Molecular self-assembly from building blocks synthesized on a surface in ultrahigh vacuum: kinetic control and topo-chemical reactions. *ACS Nano* **2**, 651 (2008)

38. Laffrentz, L., Eberhardt, V., Dri, C., Africh, C., Comelli, G., Esch, F., Hecht, S., Grill, L.: Controlling on-surface polymerization by hierarchical and substrate-directed growth. *Nature Chem.* **4**, 215 (2012)
39. Anderson, S., Anderson, H.L., Sanders, J.K.M.: Expanding roles for templates in synthesis. *Acc. Chem. Res.* **26**, 469 (1993)
40. Thompson, M.C., Busch, D.H.: Reactions of coordinated ligands. IX. Utilization of the template hypothesis to synthesize macrocyclic ligands *in situ*. *J. Am. Chem. Soc.* **86**, 3651 (1964)
41. Sprafke, J.K., Kondratuk, D.V., Wykes, M., Thompson, A.L., Hoffmann, M., Drevinskas, R., Chen, W.-H., Yong, C.K., Kärnbratt, J., Bullock, J.E., Malfois, M., Wasielewski, M.R., Albinsson, B., Herz, L.M., Zigmantas, D., Beljonne, D., Anderson, H.L.: Belt-shaped π -systems: relating geometry to electronic structure in a six-porphyrin nanoring. *J. Am. Chem. Soc.* **133**, 17262 (2011)
42. Lin, T., Shang, X.S., Adisojojoso, J., Liu, P.N., Lin, N.: Steering on-surface polymerization with metal-directed template. *J. Am. Chem. Soc.* **135**, 3576 (2013)
43. Adisojojoso, J., Li, Y., Liu, J., Liu, P.N., Lin, N.: Two-dimensional metallo-supramolecular polymerization: toward size-controlled multi-strand polymers. *J. Am. Chem. Soc.* **134**, 18526 (2012)
44. Nagahama, S., Matsumoto, A.: Two-dimensional polymer synthesis through the topochemical polymerization of alkylenediammonium muconate as a multifunctional monomer. *J. Polym. Sci. Part A: Polym. Chem.* **42**, 3922 (2004)

<http://www.springer.com/978-3-319-26598-8>

On-Surface Synthesis

Proceedings of the International Workshop On-Surface
Synthesis, École des Houches, Les Houches 25-30 May
2014

Gourdon, A. (Ed.)

2016, VIII, 287 p. 140 illus., 128 illus. in color.,

Hardcover

ISBN: 978-3-319-26598-8